Decadal-scale climate forcing of Alpine glacial hydrological systems

Lane Stuart, N (Orcid ID: 0000-0002-6077-6076)

Decadal-scale climate forcing of Alpine glacial hydrological systems

S.N. Lane[1] and P.W. Nienow[2]

1   Institute of Earth Surface Dynamics, University of Lausanne, Switzerland

2   School of GeoSciences, University of Edinburgh, U.K.

Key points

- A Shannon Entropy Index is used to quantify changing daily hydrograph shape for 6 high altitude Alpine basins, with a range of degrees of glacier cover, between 1969 and 2014.
- For the 5 most glaciated basins, there has been an increase in the frequency and amplitude of diurnal discharge fluctuations since the onset of more rapid warming in the 1980s.
- These changes in diurnal discharge are driven by reduced snow buffering of ice melt and runoff resulting from declining end of winter snow depths and greater mean annual temperatures.

Plain Language Summary

River basins that have a high proportion of ice cover are particularly sensitive to climate warming. Daily variations in insolation and temperature typically lead to fluctuations in snow and/or ice melt and thus a daily rise and fall in river flow. Snow, and the glaciers themselves, can buffer this rise and fall. For 6 high mountain Alpine basins, we show that daily discharge fluctuations are changing due to climate warming at the decadal scale, with both increasing daily discharge maxima and reducing daily discharge minima. These changes reflect decreased snow accumulation at the end of winter, reducing the buffering and increasing the onset of rapid glacier melt.

Abstract

Quantification of climate forcing of glacial hydrological systems at the decadal scale are rare because most measurement stations are too far downstream for glacier impacts to be clearly detected. Here, we apply a measure of daily hydrograph entropy to a unique set of reliable, high altitude gauging stations, dating from the late 1960s. We find a progressive shift to a greater number of days with diurnal discharge variation as well as more pronounced diurnal discharge amplitude. These changes were associated with the onset of rapid warming in the 1980s as well as declining end of winter snow depths as inferred from climate data. In glaciated catchments, lower winter snow depths reduce the magnitude and duration of snowpack buffering and encourage the earlier onset of glacier ice exposure, with associated lower surface albedo and more rapid melt. Together, these processes explain the increase in the observed intensity of diurnal discharge fluctuations.

Introduction

The impact of climate change on runoff from glacio-nival influenced river basins has been well-established at the decadal time scale, and this has provided a key conceptual understanding of the sensitivity of such basins to future climate change [Fleming & Weber, 2012]. Both snow and ice are components of the hydrological system that introduce climate memory, and thus delay the delivery of runoff downstream. Snow redistributes winter precipitation into summer runoff. Snow that survives the melt season becomes ice, thereby redistributing precipitation into runoff at some instant in the future; the timescale of this redistribution is determined by the time it takes for the ice to reach the glacier's ablation zone [Flowers, 2007]. Alpine environments have seen accelerated late 20th century and early 21st century temperature increases [Imtiaz & Miller, 2012; Kormann et al., 2015].

As a result of the sensitivity of snow accumulation and snow and ice melt to temperature rise, both nival and glacial basins are highly sensitive to temperature changes [Casassa *et al.*, 2009] and hence to the rapid warming recorded in Alpine regions in the late 20th and early 21st century. This sensitivity has been confirmed by two broad sets of observations. First, a general increase in annual runoff in basins

with significant glacial cover has been reported [e.g. Sorg et al., 2014; Huss & Hock, 2018], and associated with (a) the impacts of earlier onset of snow melt; (b) consequent earlier reduction of surface albedo; and (c) enhanced ice melt [Pellicciotti et al., 2010; Bard et al., 2015; Kormann et al., 2015]. Second, increases in runoff have been reported for the autumn [Birsan et al., 2005], winter [Birsan et al., 2005; Dery et al., 2009; Bard et al., 2015] and spring [Birsan et al., 2005, Dery et al., 2009; Bard et al., 2015, Kormann et al., 2015]. These are commonly attributed to warmer temperatures, which reduce the duration when precipitation falls as snow and may enter temporary storage.

Changes in summer runoff are more complicated because they depend on the relative degree of ice cover [Braun et al., 2000; Fleming and Clarke, 2003; Stahl & Moore, 2006; Zappa & Kan, 2007; Pellicciotti et al., 2010; Dahlke et al., 2012; Fleming & Dahlke, 2014], as ice cover influences the extent to which reductions in winter snow accumulation [Pellicciotti et al., 2010] and earlier loss of snow cover are compensated by increased summer ice melt [Zappa & Kan, 2007]. Basin intercomparisons have shown that this compensation means that late-summer runoff has a stronger positive trend in glacial than non-glacial basins in response to temperature rise [Fleming & Dahlke, 2014], and that warming impacts [Braun et al., 2000] and parabolic teleconnections [where a given forcing can have opposing effects in different locations; Dahlke et al., 2012; Fleming & Dahlke, 2014] are particularly pronounced in glacial basins through the effects of temperature on ice melt. Through time, it has been argued that temperature driven summer ice melt will enhance runoff to the point at which "peak water" is reached [Sorg et al., 2014; Huss & Hock, 2018], where after the increase in runoff due to increasing per unit area glacier melt rates become constrained and eventually counter-balanced by a declining glacier surface area [Braun et al., 2000; Jansson et al, 2003; Stahl & Moore, 2006; Casassa et al., 2009; Nolin et al., 2010; Farinotti et al., 2012; Frans *et al.*, 2016; Moyer *et al.*, 2016] and potentially, the insulating effects of increasing debris cover [e.g. Collier et al., 2015; Vincent et al., 2016].

The importance of solar radiation for both snow and ice melt means that glaciated basins commonly have a diurnal discharge hydrograph [Röthlisberger & Lang, 1987]. Melt of snow or ice on a glacier surface may then pass through a series of stores,

each of which may delay transmission to the proglacial stream [e.g. Covington et al., 2012], including the snowpack [Jansson et al, 2003], firn [e.g. Fountain, 1992], englacial channels [Fountain and Tangborn, 1985] and subglacial drainage systems [Nienow et al., 1998; Jobard & Dzikowski, 2006; Flowers, 2008; Schuler & Fischer, 2009]. Each of these stores may then influence the form of diurnal discharge hydrographs [Swift et al, 2005; Covington et al., 2012]. Snow-line recession up glacier through the melt season should enhance surface melt rates through reductions in surface albedo [Fountain & Walder, 1998] while also reducing the proportion of flow that passes through the snow pack leading to reduced flow attenuation [Fountain, 1996]. Similarly, subglacial drainage systems are commonly observed to have slower (distributed) and faster (canalised or conduit dominated) drainage components, the latter developing as a function of growing inputs of surface melt during the summer months as the snow line migrates up glacier [e.g. Nienow et al., 1998]. Research suggests that the form of the subglacial drainage system will play an important control on hydrograph shape [Flowers, 2007]. Conduits, in particular, may reduce flow attenuation because their ability to transmit water is high [Covington et al., 2012], except when glacier surface melt rates are low, resulting conduit discharges are low, and roughness effects can lead to significant flow attenuation [Gulley et al., 2012].

It is not surprising, given the above, that the lag between peak upstream melt of snow/ice and peak proglacial stream discharge declines progressively through the summer ablation season [e.g. Fountain, 1992; Jobard & Dzikowski, 2006], following up-glacier snow line recession [e.g. Nienow et al., 1998; Willis et al., 2002; Swift et al., 2005]. Given the observation that climate warming is leading to the earlier and more rapid onset of snow melt in glaciated basins, and that reduced snow cover, for a range of reasons, should lead to the earlier and more rapid onset of ice melt, it might be expected that there will also be a progressive evolution of hydrograph shape, manifest in an increase in the number of days with diurnal discharge variation, and of increasing amplitude. However, to date, almost all studies of the evolution of hydrograph shape have been conducted at the seasonal scale, at most extending to two or three melt-seasons. There are no decadal-scale studies of how hydrograph shape in heavily glaciated basins is evolving in response to climate warming even though such evolution may be a key diagnostic of the hydrological

response of such basins, in addition to measures of annual runoff [e.g. Lundquist & Cayan, 2002; Mutzner et al., 2015]. The challenge, however, is the need to have long (multi-decadal) records of sub-daily discharge, from sites proximal to glacier outlets. Multi-decadal records are needed to distinguish short-term variability from longer-term evolution, while proximity to glacier outlets is important to minimise both flow attenuation and the runoff contributions from non-glaciated parts of the basin.

In this paper, we present a unique 46-year dataset based upon 15 minute records of streamflow for the period 1969 to 2014 from 6 glaciated basins, all with reliable stream gauges located at most 2 km from the glacier snout. The geographical coverage of the basins is small (they fall within an area of 37 km^2) such that each basin is subjected to effectively the same synoptic climatic forcing. The responses that we quantify therefore reflect the internal operation of basins with different hydrological filters but subject to the same climate forcing. Work has identified the importance of objective quantification of hydrograph shape in proglacial streams [e.g. Hannah et al, 1999; Lafreneire & Sharp, 2003; Swift et al, 2005; Jobard & Dzikowski, 2006; Cauvy-Fraunié et al., 2014]. Here we apply the Shannon entropy as a means of describing hydrograph shape following its application in hydrograph quantification in non-glaciated basins [e.g. Amorocho & Espildora, 1973; Krasovskaia, 1997; Maruyama *et al.*, 2005; Pan et al., 2011; Fleming & Weber, 2012; Mokhopadhyay & Khan, 2015]. We use these entropy measures to test the hypothesis that climate warming is leading to a systematic and measurable change in the discharge hydrographs found in glaciated basins.

Methods and data sources

Study region

Figure 1 shows and Table 1 describes the characteristics of the 6 basins considered in this paper which are all part of the Grande Dixence SA hydroelectric power scheme in south-west Switzerland. The basins vary in size across one order of magnitude, and in their percentage of ice cover close to the start of the study period from 31% to 90%. Micheletti et al. [2015] provide a summary of the recent climate history of the region from the mid 1960s to present for the Col Grand Saint Bernard

(GSB, c. 28.5 km to the west south-west and 2461 m a.s.l.). As has been reported elsewhere [e.g. Costa et al., 2018], it shows a cooler period up until the mid 1980s, followed by a rapid increase in mean annual air temperature of more than $1^{o}C$ from the mid 1980s to the mid 1990s and more slowly since then.

Hydrological data

To meet regulatory requirements, since the start of hydroelectric power production, the operating company has provided precise details of the amount of water abstracted from the system to the regulatory authorities. Each basin has a water intake with a calibrated water level recorder, initially derived using a chart recorder to provide water level, and subsequently with a pressure transducer and digital data logging. Water levels are measured across a broad-crested weir with a known hydraulic function, thereby providing very reliable records of discharge (precise to ±0.01 $m^{3}s^{-1}$, for regulatory reasons, LEaux, 1991)). Data are available from 1969 with a 15 minute resolution.

Our analysis assumes that as the glaciers retreat, there is no systematic change in attenuation due to the growing distance to the proglacial margin. We believe this to be acceptable as the distances between the gauges are very short (Table 1). The Haut Glacier d'Arolla has the longest snout to gauge distance (2 km in 2014) and also the lowest proglacial area slope, and so it has the hydrographs most likely to be impacted upon by glacier recession (about 1 km between 1968 and 2014). Perolo et al. (2019) measured the travel time between the snout of the Haut Glacier d'Arolla and its gauge (Figure 1) in 2015 and found this to be about 15 to 20 minutes for both high and low flows. Thus, the effect of recession of 1 km is a travel time change (7.5 minutes) of about half a data time step (15 minutes). We argue that this will have a negligible effect on flow attenuation due to the retreating proglacial margin, an effect that will be even lower in magnitude for the other 5 glaciers studied, and that this justifies the assumption we make.

The only data processing required to enable our hydrograph analyses is the removal of drawdown events associated with flushing of the gauging station intake to remove

sediment. The duration of draw down ranges between 2 and 6 measurement periods (30 to 90 minutes). This was undertaken visually following the method described in Lane et al. (2017). After data removal, missing data were interpolated linearly, aided by the relatively smooth discharge response of these catchments. For one intake, Vuibé, data were not available from the 31st August to 31st December 2011 due to construction work on the intake.

Description of hydrograph form

The Generalised Entropy (Shannon) Index for each diurnal hydrograph (*j*) was calculated from :

$$E_j = \frac{1}{n} \sum_{i=1}^{n} \frac{Q_i}{\overline{Q_\iota}} \, log \, \frac{Q_i}{\overline{Q_\iota}}$$

[1]

where Q_i is the discharge for time step *i* of *n* time steps within diurnal hydrograph *j*, variable according to the estimated duration of each diurnal cycle. [1] measures the degree of deviation within each identified hydrograph from the mean discharge for that hydrograph. A higher value of E_j can reflect either an increase in the magnitude of the daily discharge peak and or a decrease in the magnitude of the daily discharge minimum and thus reflects increasing diurnal discharge amplitude.

Application of (1) requires the identification of diurnal hydrographs prior to its utilisation. With 6 basins and 46 years of data, this implies over 100,000 potential hydrographs, and so identification requires automation. For each basin and for each day, the flow minimum was identified. The minimum was commonly during the early morning but, at the start and end of each melt season, as well as during cold periods, it was possible that there was no distinct flow minimum on a given day. In this case, the hydrograph was not labelled as 'diurnal' and was excluded from the analysis. Where the time between hydrograph minima identified fell outside of the range of 21 to 27 hours it was manually checked and removed when the flow variation was not diurnal. A values of E_j was generated for each identified diurnal

cycle for each basin in the period 1969 to 2014 using (1). The duration of each diurnal cycle defined the number of discharge measurements used and hence n in (1). Initial inspection of the results noted some extreme values of E_j, associated with near zero flow minima, and almost exclusively at the very beginning of the melt season. A 95% threshold of each basins E_j distribution was used for removal. Each E_j series for individual basins was integrated across calendar years to give the total annual entropy. The latter is a combined function of the number of days showing a diurnal discharge variation as well as the level of entropy in each diurnal hydrograph. We also calculate the Entropy Intensity, that is the total annual entropy divided by the number of days with a diurnal hydrograph.

Mean annual air temperature and modelled snow cover

We use the GSB temperature data as representative of mean annual air temperature. We use this in preference to some combination of spring, summer and autumn temperature because the latter require a-priori definition of a start and end date when there will in fact be considerable interannual variability in when a particular season starts. We also were interested in the history of snow cover in each basin. Long time series of both solid precipitation and accumulated snow depth are however rare, and almost unheard of for glaciers. Daily snow depth data were available for Fontanesses (Figure 1), a measurement site just to the north-west of Glacier de Tsijiore Nouve at 2'850 m above sea level from 1998 to 2011. We needed to extrapolate these to the altitudinal ranges for the 6 glaciers in our study. To do this, we used the modelled snow cover data from Micheletti *et al.* [2015], where full details can be found. Micheletti et al. used a parsimonious model, GSM-SOCONT (Glacier and SnowMelt - SOil CONTribution model, Schaefli et al. [2005]) to produce long time-series of daily snow depth for altitudinal bands for the region. GSM-Socont is a semi-distributed glacial-hydrological model that simulates daily snow cover and runoff from mountain catchments. Snow melt is based on the degree-day approach [e.g. Hock, 1999]. We used available temperature and precipitation data from proximate stations (Sion and Hérémence) and optimised both empirical lapse rates for temperature, precipitation and snowfall using the Fontanesses data. After calibration, the daily mean error for Fontanesses was 8.6 cm with a precision of ±38.2 cm at the 90% confidence level. The model was then used to provide

predictions for 10 m altitudinal bands. It should be emphasised that this approach has some uncertainties (e.g. the lapse rate calculations) but we assume that the patterns that the modelled snow data provide are sufficient to elucidate general rather than detailed forcing of hydrograph response due to snow cover.

Given the significance of snow line recession for glacier melt and runoff characteristics [Nienow et al., 1998; Willis et al, 2002], we determined for each year two parameters. First, we determined the mean snow depth at the end of the winter for each glacier terminus (here taken as 31st March). Under the assumption that snow depth increases with altitude, this was chosen as a measure of the minimum depth of snow that has to be melted before lower albedo glacier ice becomes exposed and enhanced melt and reduced snowpack attenuation effects begin. We use the 31st March as the end of winter date, following Marty and Meister (2012, their Figure 7), who show for 51 Swiss snow measurement stations with a median altitude of 2'405 m above sea level (i.e. comparable to the margins of the glaciers studied here) that this provides a rough approximation of when snow accumulation ends. Second, we use the altitude distribution for each glacier derived from the 2009 glacier extents [Fischer et al., 2014] to estimate the percentage of the glacier that was snow covered at what is approximately the end of the ablation season for European glaciers, the 30th September. Marty and Meister (2012) also show that September-October is a period of largely stable snow cover.

We explore the relationships between annual entropy/entropy intensity and air temperature, March snow cover and September snow cover using correlation and partial correlation. The analyses show the importance of the partial correlation and the relationships revealed for air temperature and March snow cover. In order to aid visualisation of the partial correlations, we : (a) plot annual entropy/entropy intensity against air temperature; and (b) plot the residuals of the linear fit between entropy/entropy intensity against air temperature and against March snow cover. The latter are a close approximation to the partial correlations.

Results

Figure 2 shows an example of the daily entropy values and the associated discharge time-series for the year 1990 for the Haut Glacier d'Arolla. Following Nienow et al. [1998], in 1990 by the 23rd June, the snow line had retreated 0.7 km upstream from the snout margin and most (>85%) of the glacier was snow covered. Diurnal discharge variation to this date was small with proportionately high minimum flows. The E_j values were low. E_j values then increase steadily to early August: first, due to increasing peak flows but whilst baseflows remain relatively high; then from the middle of July, after which peak flows approximately stabilise, due to a fall in baseflow. In parallel, the snowline retreated between the end of June (c. 0.75 km) to 3.60 km by the end of July [Nienow et al., 1998] associated with greater hydrological efficiency in response to snow line recession (with less than 90% of the glacier snow covered by the end of July). The trend of increasing E_j continues to a maximum on 13th August, which is not the day with the highest discharge (3rd August) but has a relatively high discharge maximum followed by a very low discharge minimum. Indeed, from August onwards there is substantial variability in E_j values reflecting the relative size of discharge maxima and minima. From the 1st September onwards, there is a general decline in E_j caused primarily by a greater rate of decline in peak flow rather than baseflow.

Figure 3 shows E_j through time for each year from 1969-2014. For all of the basins except Douves Blanches, there is: (1) a general tendency for E_j to increase with time within each specific year; and (2) a late melt season increase in entropy (from around the middle of July) in the late 1980s and early 1990s, although for Tsijiore Nouve this is only clear from the 2000s. The total annual entropy (Figure 4) is at a minimum in all basins except Douves Blanches around 1980, followed by two periods (late 1980s to mid 1990s; mid 2000s) of higher annual entropy for Bertol, Haut Glacier d'Arolla, Vuibé and Pièce. Five year running means (Figure 4) suggest two peaks in annual entropy in the late 1980s or early 1990s and the 2000s, except for Tsijiore Nouve where the first peak is in the late 1990s. Entropy intensity patterns (Figure 4) are similar to total entropy (Figure 4) suggesting that the annual entropy scales with the number of days on which diurnal discharge cycles were identified. A Mann-Kendall test suggests that the trend in total annual entropy is significant

($p<0.05$) for all glaciers except Douves Blanches and that the trend in entropy intensity is significant ($p<0.05$) for all glaciers, albeit negative rather than positive for Douves Blanches.

Table 2 shows the correlations (Table 2a) and partial correlations (Table 2b) between annual entropy, entropy intensity, and basic climate parameters. The correlations suggest that, with the exception of Douves Blanches, annual entropy and entropy intensity are both driven by mean annual air temperature (MAAT), late March snow depth at the glacier margin and the percentage of each glacier that is snow-covered in late September (Table 2a). However, as there is also some inter-correlation, partial correlation (Table 2b) is needed to isolate the relationships between variable pairs. Excluding Douves Blanches, the basin with the lowest percentage ice cover (Table 1), partial correlations between temperature and both entropy measures are lower, but still significant, in all cases (see also Figures 5 and 6). More interestingly, the partial correlations between both entropy measures and September glacier snow cover are no longer significant; whilst those between both entropy measures and the end of March snow depth remain significant (see also Figures 5 and 6). It appears therefore that entropy is driven by: (1) the snout snow depth at the end of March which reflects winter precipitation, normally solid at these snout altitudes; greater snout snow depth leads to lower annual entropy and entropy intensity; and (2) the mean annual air temperature which represents the intensity of melt and hence the percentage of the glacier that is snow covered at the end of September. With the exception of the Bertol glacier, the magnitudes of significant partial correlations between annual entropy and mean annual air temperature are greater than the partial correlations of annual entropy with 31st March snow depth. In contrast, and with the exception of Tsijiore Nouve and Vuibé, the magnitude of significant partial correlations between entropy intensity with 31st March snow depth are greater than with mean annual air temperature. Thus, there is some evidence that mean annual air temperature drives the number of days when there is diurnal discharge variation, but the 31st March snow depth (and thus control on the rate of snowline retreat) drives the magnitude of diurnal discharge fluctuations during the summer that follows.

Figure 7 shows a time-series of 31st March snow depth and mean annual air temperature, between 1969 and 2014. Temperature has increased significantly throughout the period (Mann-Kendall test, $p<0.05$). The snow depth record is more complicated, with a marked increase to the 1980s, and a significant negative trend (Mann-Kendall, $p<0.05$) from 1981 onwards, but not at the scale of the whole period (1969-2014). The entropy patterns (Fig. 3 and 4) reflect these changes. For the five basins showing significant partial correlations (Table 2b), a series of higher 31st March snow depths at the end of the 1970s and the beginning of the 1980s is reflected in lower levels of annual entropy and entropy intensity (Fig. 4). From the mid 1980s, there is a rapid increase in mean annual air temperature (Fig. 7) which is reflected in the increasing annual entropy and entropy intensity (Fig. 4). In the mid to late 1990s, mean annual temperature falls slightly and 31st March snow cover increases slightly, and this coincides with small entropy falls for all five basins (Fig. 4), albeit to a reduced degree for Tsijiore Nouve. Finally, since the mid 2000s, low levels of 31st March snow cover in combination with some of the highest MAAT result in some of the highest levels of entropy (Fig. 4 and 7).

Implications

We have presented the first multi-decadal analysis of the form of daily discharge hydrographs for a set of small Alpine glaciated basins, all of which are being forced by the same climatic signal. The analysis suggests a pronounced climatic forcing of hydrograph shape in five of the six basins (Table 2) with a general transition since the mid-1980s to both stronger diurnal discharge variability and more days when diurnal discharge variation is present (Fig. 2). Our findings demonstrate that the forcing had two elements: (1) the depth of snow accumulated during winter, which controls the amount of snow that must be melted before the onset of lower albedo ice-melt can begin, and which after an early 1980s peak has been in decline (Figure 7; see also Pellicciotti et al., [2010]); and (2) the mean annual air temperature. This is the first study that shows that climatic warming and changing preservation of solid precipitation over winter have combined to produce diurnal hydrographs both on more days during the year and of greater amplitude.

The importance of end of winter snow cover is not surprising, because it is well established that snow cover reduces glacial melt [Fountain & Walder, 1998; Willis et al, 2002], delays runoff [Fountain, 1996; Hannah & Gurnell, 2001; Campbell et al., 2006], and slows the development of more efficient subglacial drainage systems [Nienow et al., 1998]. Snowmelt from non-glaciated parts of a basin will also contribute to the diurnal discharge variation (May and early June, Figure 2) but, whether from the glaciated or non-glaciated parts of the basin, runoff during this period is damped by both the higher albedo and the effects of the snowpack upon the flux of melt to the basin outlet.

Whilst entropy fell for the five most glaciated basins during the early 1980s (Figure 4), when snow depths at the end of winter were typically higher (Figure 7), and then rose again with falling March snow cover and rising temperature from the 1980s (Figure 7), this was not the case for Douves Blanches. This suggests that below a critical percentage glacier cover, the impacts of ice melt on diurnal discharge variation become less apparent. This decline in cover may be due to glacier recession or the progressive accumulation of debris on the glacier surface. Research has shown that melt rates are enhanced up until a certain thickness due to reduced albedo, but then the albedo enhancing effects of debris cover become progressively countered by the time it takes for the debris to conduct heat through to the ice surface hence the insulating effect of the debris reduces melt. The classic study of Östrem (1959) at Isfallglaciären in Iceland suggested a critical thickness of 5 mm, with melt rates declining thereafter as debris thickness increased. Subsequent field [e.g. Clark et al., 1994; Collier et al., 2015; Vincent et al., 2016], laboratory [e.g. Nakawo & Young, 1992] and modelling [e.g. Evatt et al., 2015; Carenzo et al., 2016] studies have confirmed the general form of this curve. They have also shown that the critical thickness and the specific decay of melt rate with debris thickness vary with the duration of solar radiation, season, local slope aspect and debris characteristics [e.g. Nicholson & Benn, 2013; Gibson et al., 2018]. Whether the decline in glacier ice surface exposure is due to glacier retreat or debris driven ice insulation, it suggests that beyond a critical level of glacier cover, a basin should transition to reduced intensity of diurnal variation (Douves Blanches, Figure 4) and independence between temperature/snow cover and the intensity of diurnal discharge variation (Douves Blanches, Table 2, Figures 5 and 6). Thus, the temporal

evolution of the annual entropy and its intensity may be a valuable diagnostic of the extent to which the ice melt subsidy of annual runoff in glaciated basins is changing. In terms of annual runoff, this has been described as "peak water" [e.g. Sorg et al., 2014; Huss & Hock, 2018], and it is commonly addressed through quantification of changes in annual runoff [e.g. Huss et al., 2008]. However, annual runoff may also contain a precipitation signal (for example a reduction in winter snow accumulation [e.g. Pellicciotti et al., 2010; Bard et al., 2015; Kormann et al., 2015]), itself evolving as a function of climate, thereby masking the changing contribution from annual runoff. This precipitation signal is likely to become stronger as glacier cover declines.

These results have potentially important implications for the management of hydropower systems. More frequent and stronger diurnal discharge fluctuations are likely to increase subglacial sediment evacuation significantly (Swift et al, 2005) thereby explaining observed increases in sediment delivery to hydropower intakes [Micheletti & Lane, 2016; Lane et al., 2017]. Climatically driven changes in hydrograph shape also help to explain the long-established model of paraglacial response of deglaciating basins [Church & Ryder, 1972]; during deglaciation, sediment yield rises rapidly, before declining as the percentage of a basin that is ice covered falls. Whilst the progressive stabilisation of the landscape (e.g. through sediment sorting processes) might explain this decline, it could also be due to the progressive loss of sediment transport capacity once the percentage of a basin that is glaciated has fallen below a certain threshold. The annual entropy for Douves Blanches (Figure 4) suggests that this glacier is now in such a state; indeed, Micheletti and Lane [2016] report declining sediment yield for this basin from around 2005.

depth data are freely available, under the unique identifier NM_SOCONT2015. The daily snow depth data for Fontanesses used to parameterise the snow model are freely available under license for teaching and research purposes from the Swiss Federal Government via IDAWEB (gate.meteoswiss.ch/idaweb/login.do). The temperature data for the Col du Grand Saint-Bernard are freely available from the Swiss Federal Office of Meteorology and Climatology (www.meteoswiss.admin.ch) under Climate, "Homogeneous data series since 1864".

References

Amorocho, J. & Espildora, B. (1973). Entropy in the assessment of uncertainty in hydrologic systems and models. Water Resources Research, 9, 1511-22

Bard, A., Renard, B., Lang, M., Giuntoli, I., Korck, J., Koboltschnig, G., Janza, M., d'Amico, M. & Volken, D. (2015). Trends in the hydrologic regime of Alpine rivers. Journal of Hydrology, 529, 1823-37

Birsan, M.-V., Molnar, P., Burlando, P., & Pfaundler, M. (2005). Stream- flow trends in Switzerland. Journal of Hydrology, 314, 312–329.

Braun, L.N., Weber, M., & Schulz, M. (2000). Consequences of climate change for runoff from Alpine regions. Annals of Glaciolology, 31, 19–25.

Campbell, F., Nienow, P. & Purves, R. (2006). Role of the supraglacial snowpack in mediating meltwater delivery to the glacier system as inferred from dye tracer investigations. Hydrological Processes, 20, 969-985.

Carenzo, M., Pellicciotti, F., Mabillard, J., Reid, T. & Brock, B.W. (2016). An enhanced temperature index model for debris-covered glaciers accounting for thickness effect. Advances in Water Resources, 94, 457–469

Casassa G., Lopez P., Pouyaud B., & Escobar F. (2009). Detection of changes in glacial run-off in alpine basins: examples from North America, the Alps, central Asia and the Andes. Hydrological Processes, 23, 31–41

Cauvy-Fraunié, S., Espinosa, R., Andino, P. , Dangles, O. & Jacobsen, D. (2014). Relationships between stream macroinvertebrate communities and new flood‐based indices of glacial influence, Freshwater Biology, 59, 1916-1925

Clark, D.H., Clark, M.M., & Gillespie, A.R. (1994). Debris‑covered glaciers in the Sierra Nevada, California, and their implications for snowline reconstructions. Quaternary Research, 41, 139‑153

Collier, E., Maussion, F., Nicholson, L., Mölg, T., Immerzeel, W.W. & Bush, A.B.G. (2015). Impact of debris cover on glacier ablation and atmosphere-glacier feedbacks in the Karakoram. The Cryosphere, 9, 1617 - 1632

Costa, A., Molnar, P., Stutenbecker, S., Bakker, M., Silva, T.A.A., Schlunegger, F., Lane, S.N., Loizeau, J.-L. & Girardclos, S. (2018). Temperature signal in fine sediment export from an Alpine catchment. Hydrology and Earth System Science, 22, 509-28

Covington, M.D., Banwell, A.F., Gulley, J., Saar, M.O., Willis, I.C. & Wicks, C.M. (2012). Quantifying the effects of glacier conduit geometry and recharge on proglacial hydrograph form. Journal of Hydrology, 414, 59-71

Dahlke, H.E., Lyon, S.W., Stedinger, J.R., Rosqvist, G., & Jansson, P. (2012). Contrasting trends in floods for two sub-arctic catchments in northern Sweden – does glacier presence matter? Hydrology and Earth System Sciences, 16, 2123-2141

Déry, S.J., K. Stahl, R.D., Moore, P.H. Whitfield, B., Menounos, & Burford, J.E., (2009). Detection of runoff timing changes in pluvial, nival, and glacial rivers of western Canada, Water Resources Research, 45, W04426

Evatt, G.W., Abrahams, I.D., Heil, M., Mayer, C., Kingslake, J., Mitchell, S.L., Fowler, A.C. & Clark, C.D. (2015). Glacial melt under a porous debris layer. Journal of Glaciology, 61, 825–836

Farinotti, D., Usselmann, S., Huss, M., Bauder, A. & Funk, M. (2012). Runoff evolution in the Swiss Alps: projections for selected high-alpine catchments based on ENSEMBLES scenarios. Hydrological Processes, 26, 1909–24

Fischer, M., Huss, M., Barboux, C. & Hoelzle, M. (2014). The new Swiss Glacier Inventory SGI2010: relevance of using high-resolution source data in areas dominated by very small glaciers. Arctic, Antarctic, and Alpine Research, 46, 933–945

Fleming, S.W. & Dahlke, H.E. (2014). Modulation of linear and nonlinear hydroclimatic dynamics by mountain glaciers in Canada and Norway: Results

from information-theoretic polynomial selection. Canadian Water Resources Journal, 39, 324-41

Fleming, S.W. & Weber, F.A. (2012). Detection of long-term change in hydroelectric reservoir inflows: bridging theory and practise. Journal of Hydrology, 470–471, 36–54

Flowers, G.E. (2008). Subglacial modulation of the hydrograph from glacierized basins. Hydrological Processes, 22, 3903-18.

Fountain A.G. & Walder J.S. (1998). Water flow through temperate glaciers. Reviews of Geophysics, 36, 299–328

Fountain, A. G. (1996). Effect of snow and firn hydrology on the physical and chemical characteristics of glacial runoff. Hydrological Processes, 10, 509–521, 1996

Fountain, A. G. & Tangborn, W. V (1985). The effect of glaciers on streamflow variations, Water Resource Research, 21, 579–586, 1985.

Fountain, A.G. (1992). Subglacial water flow inferred from stream measurements at South Cascade Glacier, Washington, USA, Journal of Glaciology, 38, 51-64.

Fountain, A.G. (1996). Effect of snow and firn hydrology on the physical and chemical characteristics of glacial runoff, Hydrological Processes, 10, 509-21.

Frans, C., Istanbulluoglu, E., Lettenmaier, D.P., Clarke, G., Bohn, T.J., & Stumbaugh, M. (2016). Implications of decadal to century scale glacio-hydrological change for water resources of the Hood River basin, OR, USA. Hydrological Processes, 30, 4314-29

Gibson, M.J., Irvine-Fynn, T.D.L., Wagnon, P., Rowan, A.V., Quincey, D. J., Homer, R., & Glasser, N.F. (2018). Variations in near‐surface debris temperature through the summer monsoon on Khumbu Glacier, Nepal Himalaya. Earth Surface Processes and Landforms, 43, 2698–2714.

Gulley, J.D., Walthard, P., Martin, J. & Banwell, A.F. (2012). Conduit roughness and dye-trace breakthrough curves: why slow velocity and high dispersivity may not reflect flow in distributed systems. Journal of Glaciology, 58, 915-25.

Hannah, D.M. & Gurnell, A.M. (2001). A conceptual, linear reservoir runoff model to investigate melt season changes in cirque glacier hydrology. Journal of Hydrology, 246, 123-41

Hannah, D.M., Gurnell, A.M. & McGregor, G.R. (1999). A methodology for investigation of the seasonal evolution in proglacial hydrograph form. Hydrological Processes, 13, 2603–2621.

Hock, R. (1999). A distributed temperature-index ice- and snowmelt model including potential direct solar radiation. Journal of Glaciology, 45, 101– 111.

Huss, M. & Hock, R. (2018). Global-scale hydrological response to future mass glacier loss. *Nature Climate Change*, 8, 135-40.

Huss, M., Farinotti, D., Bauder, A., & Funk, M. (2008). Modelling runoff from highly glacierized alpine drainage basins in a changing climate, Hydrological Processes, 22, 3888–3902.

Imtiaz R. & Miller, J.R. (2012). Climate change in mountains: a review of elevation-dependent warming and its possible causes. Climatic Change, 114, 527-47

Jansson P., Hock R. & Schneider T. (2003). The concept of glacier storage: a review. Journal of Hydrology. 282, 116–129

Jobard, S. & Dzikowski, M. (2006). Evolution of glacial flow and drainage during the ablation season. Journal of Hydrology, 330, 663-71.

Kormann, C., Francke, T. & Bronstert, A. (2015). Detection of regional climate change effects on alpine hydrology by daily resolution trend analysis in Tyrol, Austria. Journal of Water and Climate Change, 6, 124-43

Krasovskaia, I. (1997). Entropy-based grouping of river flow regimes. Journal of Hydrology, 202, 173–191

Lafreneire, M. & Sharp, M. (2003). Wavelet analysis of inter-annual vari- ability in the runoff regimes of glacial and nival stream catch- ments, Bow Lake, Alberta. Hydrological Processes, 17, 1093–1118.

Lane, S.N., Bakker, M., Gabbud, C., Micheletti, N. & Saugy, J-N. (2017). Sediment export, transient landscape response and catchment-scale connectivity following rapid climate warming and Alpine glacier recession. Geomorphology, 277, 210-27

LEaux, 1991. Loi fédérale sur la protection des eaux. Confédération Helvétique, Bern, 34pp.

Lundquist, J.S. & Cayan, D.R., (2002). Seasonal and spatial patterns in diurnal cycles in streamflow in the western United States. Journal of Hydrometeorology, 3, 591-603.

Marty, C. & Meister, R. (2012). Long-term snow and weather observations at Weissfluhjoch and its relation to other high-altitude observatories in the Alps. *Theoretical and Applied Climatology*, 110, 573-83

Maruyama, T., Kawachi, T. & Singh, V.P. (2005). Entropy-based assessment and clustering of potential water resources availability. Journal of Hydrology, 309, 104-113.

Micheletti, N. & Lane, S.N. (2016). Water yield and sediment export in small, partially glaciated Alpine watersheds in a warming climate. Water Resources Research, 52, 4924–4943

Moyer, A. N., Moore, R. D., and Koppes, M. N. (2016). Streamflow response to the rapid retreat of a lake‐calving glacier. Hydrological Processes, 30, 3650–3665

Mukhopadhyay, B. & Khan, A. (2015). Boltzmann-Shannon entropy and river flow stability within Upper Indus Basin in a changing climate. International Journal of River Basin Management, 13, 87-95.

Mutzner, R., Weijs, S.V., Tarolli, P., Calaf, M., Oldroyd, H.J. & Parlange, M.B., (2015), Controls on the diurnal streamflow cycles in two subbasins of an alpine headwater catchment, Water Resour. Res., 51, 3403–3418

Nakawo, M. & Young G.J. (1982). Estimate of glacier ablation under a debris layer from surface temperature and meteorological variables. Journal of Glaciology 28: 29–34

Nicholson, L. & Benn, D.I. (2013). Properties of natural supraglacial debris in relation to modelling sub‐debris ice ablation. Earth Surface Processes and Landforms, 28, 490‐501

Nienow, P. , Sharp, M. & Willis, I. (1998). Seasonal changes in the morphology of the subglacial drainage system, Haut Glacier d'Arolla, Switzerland. Earth Surface Processes and Landforms, 23, 825-843

Nolin, A.W., Phillippe, J., Jefferson, A. & Lewis, S.L. (2010). Present-day and future contributions of glacier runoff to summertime flows in a Pacific Northwest watershed: Implications for water resources. Water Resources Research, 46, W12509

Östrem, G. (1959). Ice melting under a thin layer of moraine, and the existence of ice cores in moraine ridges. Geografiska Annaler, 41, 228–230.

Pan, F., Pachepsky, Y.A., Guber, A.K., & Hill, R.L. (2011). Information and complexity measures applied to observed and simulated soil moisture time series. Hydrological Sciences Journal, 56, 1027–1039

Pellicciotti, F., Bauder, A. & Parola, M. (2010). Effect of glaciers on streamflow trends in the Swiss Alps. Water Resources Research, 46, W10522

Perolo, P., Bakker, M., Gabbud, C., Moradi, G., Rennie, C., & Lane, S.N. (2019), Subglacial sediment production and snout marginal ice uplift during the late ablation season of a temperate valley glacier. Forthcoming in Earth Surface Processes and Landforms

Röthlisberger, H. & Lang, H. (1987). Glacial Hydrology. In A.M. Gurnell and M.J. Clark (Eds), Glaciofluvial sediment transfer : an Alpine perspective, Wiley, Chichester, 207-84

Schuler, T.V., & Fischer, U.H. (2009). Modeling the diurnal variation of tracer transit velocity through a subglacial channel, Journal of Geophysical Research – Earth Surface, 114, F04017.

Sorg, A., Huss, M., Rohrer, M. & Stoffel, M. (2014). The days of plenty might soon be over in glacierized Central Asian catchments. Environmental Research Letters, 9, 104018

Stahl, K. & Moore, R.D. (2006). Influence of watershed glacial coverage on summer streamflow in British Columbia, Canada. Water Resources Research, 42, W05022

Swift, D., Nienow, P., Hoey, T. & Mair, D. (2005). Seasonal evolution of runoff from Haut Glacier d'Arolla, Switzerland and implications for glacial geomorphic processes. Journal of Hydrology, 309, 133-148

Vincent, C., Wagnon, P., Shea, J., Immerzeel, W., Kraaijenbrink, P., Shrestha, D., Sorunco, A., Arnaud, Y., Brun, F., Berthier, E., Sherpa, S. (2016). Reduced melt on debris‑covered glaciers: investigations from Changri Nup Glacier, Nepal. *The Cryosphere*, 10, 1845‑1858

Willis, I., Arnold, N. & Brock, B. (2002). Effect of snowpack removal energy balance, melt and runoff in a small supraglacial basin. Hydrological Processes, 16, 2721–2749.

Zappa, M. & Kan, C. (2007). Extreme heat and runoff extremes in the Swiss Alps. Natural Hazards and Earth System Sciences, 7, 375-389

Table 1. Basic characteristics of each basin. Basin sizes from gauging station sheets (Grande Dixence SA). % glaciated based on glacier surface area from the 2009 GLIMS data base for Switzerland (Fischer et al., 2014), except for Vuibé which uses 1973 data from Grande Dixence and for which data are not available for 2009. Maximum altitude defined by bergschrund height from 2014 aerial imagery; terminus altitude is from 2014 field mapping. Data for Vuibé are not in the GLIMS record and so were digitized manually from the closest available date.

Parameter	Bertol	Douves Blanches	Haut Glacier d'Arolla	Vuibé	Pièce	Tsijiore Nouve
Basin size upstream of gauge (km^2)	2.51	1.01	12.65	2.27	2.79	4.77
% glaciated in 1973	21.9	21.8	45.9	90.0	52.8	67.0
% glaciated in 2009	13.6	6.9	27.2	NA	45.1	57.1
1973 snout altitude (m a.s.l.)	2840	2980	2560	2700	2630	2223
1973 glacier mean altitude (m a.s.l.)	3080	3220	2960	3600	2911	3300
1973 glacier maximum altitude (m a.s.l.)	3300	3360	3480	3795	3695	3770
Aspect	SW	SW	N	NE	N	NNE
Gauge distance from snout, 1973 (km)	0.90	0.94	1.15	0.16	0.35	0.47
Gauge distance from snout 2014 (km)	1.37	1.35	1.99	0.66	0.60	0.82

Table 2. Correlations (Table 2a) and partial correlations (Table 2b) between basic climatic parameters and annual entropy and entropy intensity for the 6 glaciers considered. * indicates significant at $p<0.05$, using a one-directional test of correlation with the sign of the tested association indicated in brackets in the first column and $n-2$ degrees of freedom (correlation) and n-4 degrees of freedom (partial correlation). Data for 2011 for Vuibé are excluded due to the gauge being out of order from the 30th August.

2a

	MAAT (GSB)	31st March snow depth	30th September % glacier snow covered		MAAT GSB	31st March snow depth	30th September % glacier snow covered
Bertol							
Annual Entropy	**0.49***	**-0.63***	**-0.39***	Entropy Intensity	**0.39***	**-0.54***	**-0.39***
MAAT (GSB)		-0.18	**-0.46***	MAAT (GSB)		-0.18	**-0.46***
31st March snow depth			**0.26***	31st March snow depth			**0.26***
Douves Blanches							
Annual Entropy	0.16	-0.12	-0.07	Entropy Intensity	-0.34	-0.06	0.19
MAAT (GSB)		-0.18	**-0.46***	MAAT (GSB)		-0.18	**-0.46***
31st March snow depth			**0.26***	31st March snow depth			**0.26***
Haut Glacier d'Arolla							
Annual Entropy	**0.62***	**-0.52***	**-0.42***	Entropy Intensity	**0.45***	**-0.43***	**-0.37***
MAAT (GSB)		-0.16	**-0.54***	MAAT (GSB)		-0.16	**-0.54***
31st March snow depth			0.16	31st March snow depth			0.16
Glacier de Vuibé							
Annual Entropy	**0.62***	**-0.29***	**-0.39***	Entropy Intensity	**0.66***	**-0.26***	**-0.47***
MAAT (GSB)		-0.16	**-0.51***	MAAT (GSB)		-0.16	**-0.51***
31st March snow depth			0.17	31st March snow depth			0.17
Glacier de Pièce							
Annual Entropy	**0.58***	**-0.42***	**-0.49***	Entropy Intensity	**0.51***	**-0.45***	**-0.41***
MAAT (GSB)		-0.16	**-0.54***	MAAT (GSB)		-0.16	**-0.54***
31st March snow depth			0.12	31st March snow depth			0.12
Glacier de Tsijiore Nouve							
Annual Entropy	**0.52***	**-0.34***	**-0.33***	Entropy Intensity	**0.38***	**-0.31***	**-0.28***
MAAT (GSB)		-0.17	**-0.54***	MAAT (GSB)		-0.17	**-0.54***

31st March snow depth			0.19	31st March snow depth			0.19

2b

|	MAAT (GSB)	31st March snow depth	30th September % glacier snow covered		MAAT GSB	31st March snow depth	30th September % glacier snow covered
Bertol							
Annual Entropy	**0.41***	**-0.61***	-0.12	Entropy Intensity	**0.27***	**-0.50***	-0.18
MAAT (GSB)		0.20	**-0.35***	MAAT (GSB)		0.08	**-0.36***
31st March snow depth			0.09	31st March snow depth			0.09
Douves Blanches							
Annual Entropy	0.14	-0.10	0.02	Entropy Intensity	-0.29	-0.01	0.04
MAAT (GSB)		-0.05	**-0.43***	MAAT (GSB)		-0.07	**-0.40***
31st March snow depth			0.20	31st March snow depth			0.20
Haut Glacier d'Arolla							
Annual Entropy	**0.55***	**-0.54***	-0.10	Entropy Intensity	**0.32***	**-0.40***	-0.14
MAAT (GSB)		0.23	**-0.38***	MAAT (GSB)		0.05	**-0.45***
31st March snow depth			0.02	31st March snow depth			0.03
Glacier de Vuibé							
Annual Entropy	**0.59***	**-0.29***	-0.08	Entropy Intensity	**0.55***	**-0.26***	-0.19
MAAT (GSB)		0.15	**-0.34***	MAAT (GSB)		0.13	**-0.26***
31st March snow depth			0.09	31st March snow depth			0.07
Glacier de Pièce							
Annual Entropy	**0.43***	**-0.41***	-0.22	Entropy Intensity	**0.36***	**-0.43***	-0.19
MAAT (GSB)		0.08	**-0.38***	MAAT (GSB)		0.06	**-0.42***
31st March snow depth			-0.06	31st March snow depth			-0.05
Glacier de Tsijiore Nouve							
Annual Entropy	**0.43***	**-0.29***	-0.04	Entropy Intensity	**0.27***	**-0.27***	-0.07
MAAT (GSB)		0.05	**-0.45***	MAAT (GSB)		-0.01	**-0.48***
31st March snow depth			0.10	31st March snow depth			0.09
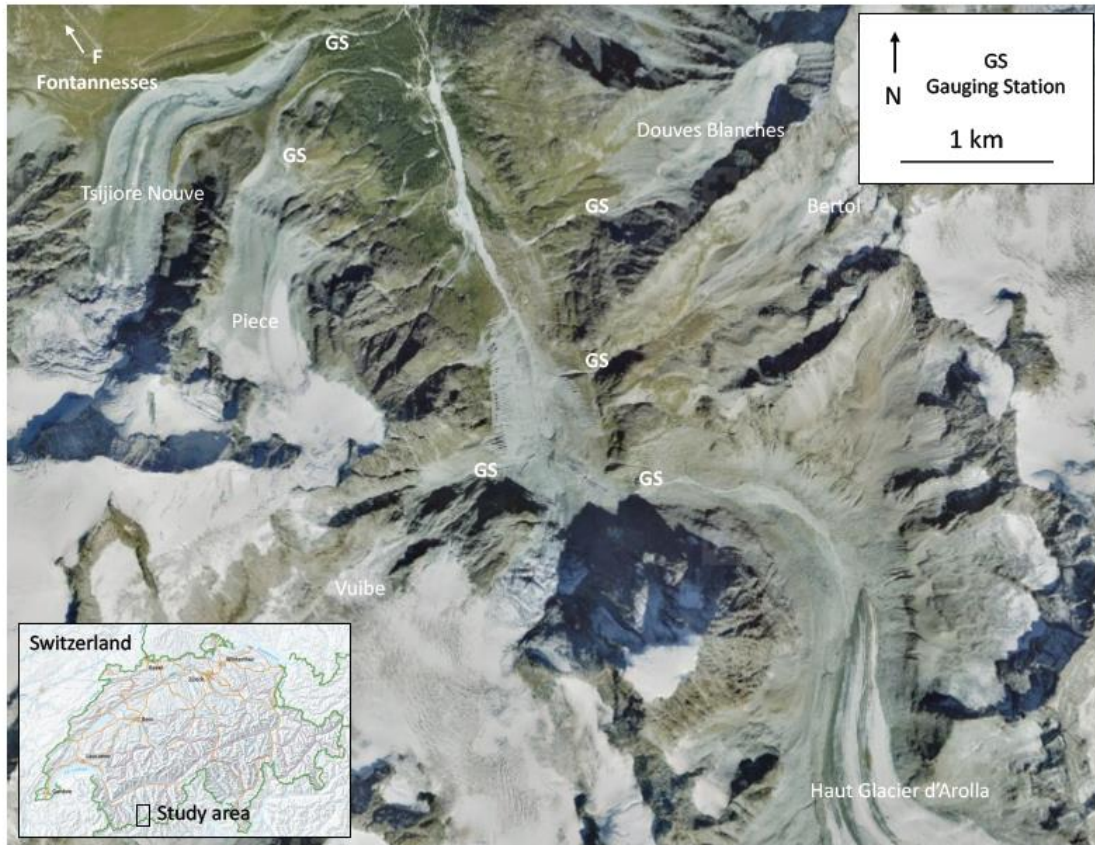
Figure 1. The study basins showing the glaciers and the gauging stations and the Fontanesses site used to calibrate the snow model. The image and the inset are provided by the Swiss Federal Office of Topography, SwissTopo and can be accessed at http://map.geo.admin.ch (search on Arolla)
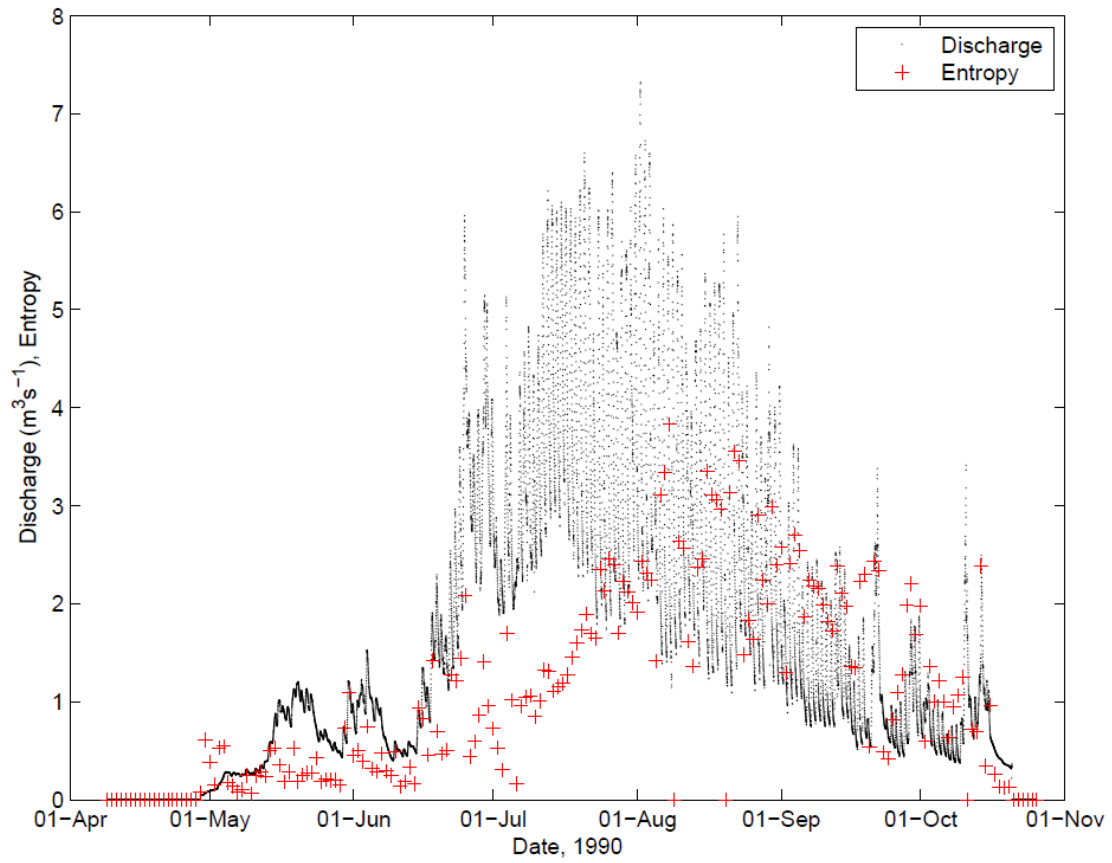
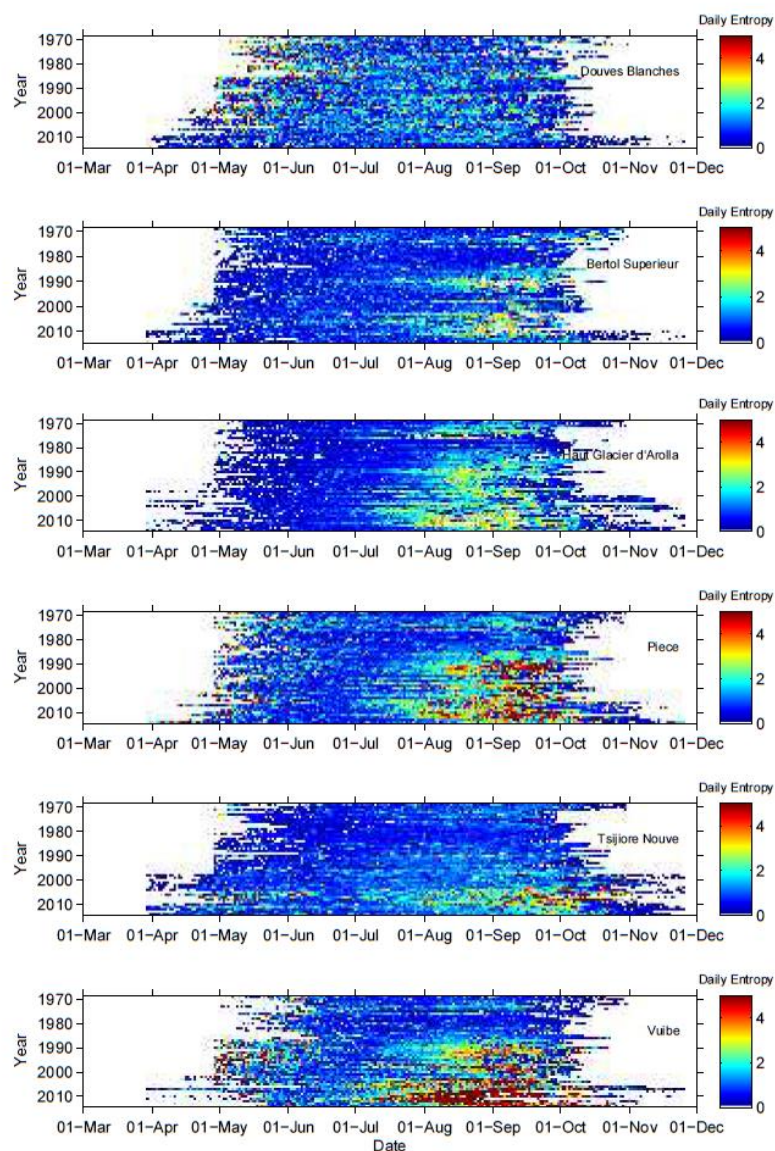Figure 2. Daily entropy values superimposed on a discharge hydrograph for the Haut Glacier d'Arolla for the year 1990.

Figure 3. Daily E_j values for the period 1969 to 2014. Only the 1st March to the 1st December are shown to aid visualisation.
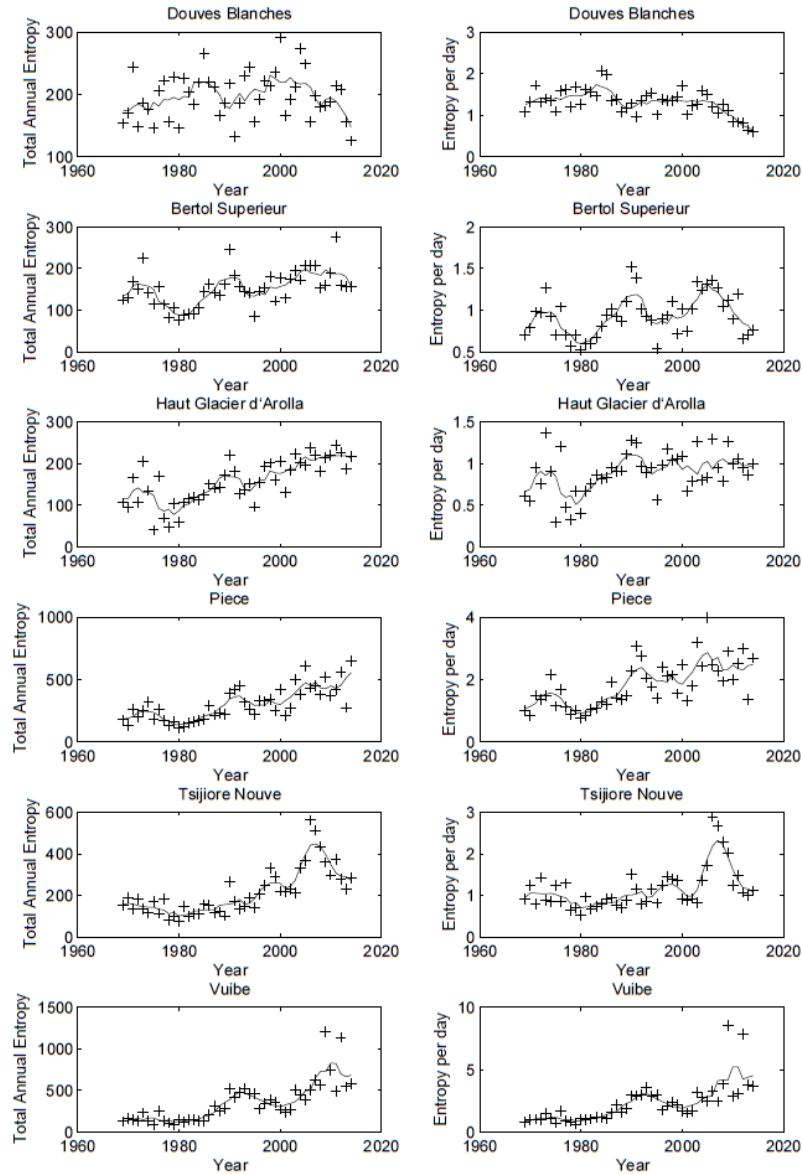
Figure 4. Annually integrated entropy and the entropy intensity (the annually integrated entropy divided by the number of days with a diurnal discharge cycle) plotted with a 5 year running mean.
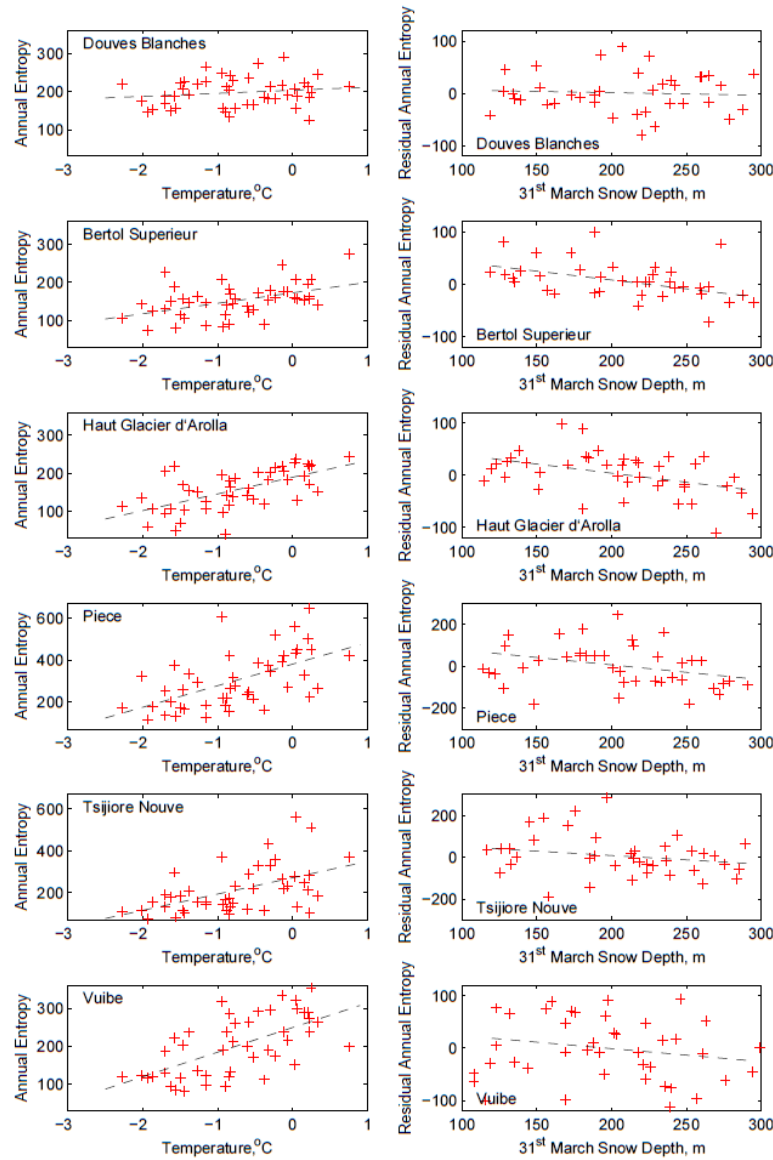
Figure 5. Plots of the annual entropy for each glacier; against Mean Annual Air Temperature (MAAT) for Grand Saint Bernard; and of the residuals from the linear fit of annual entropy versus MAAT against end of March snow cover. Residuals are defined as positive when the annual entropy is greater than that predicted by temperature. Fitted regression lines are shown.
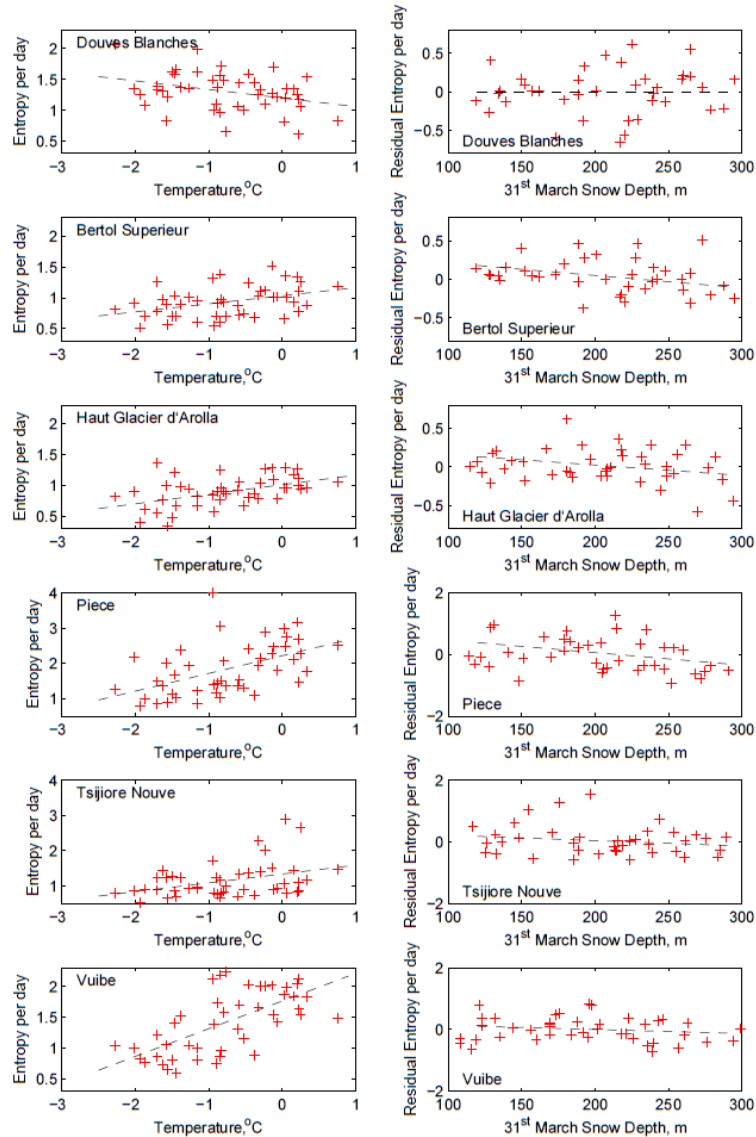
Figure 6. Plots of the entropy intensity (mean entropy per day) for each glacier; against Mean Annual Air Temperature (MAAT) for Grand Saint Bernard; and of the residuals from the linear fit of entropy intensity versus MAAT against end of March snow cover. Residuals are defined as positive when the entropy intensity is greater than that predicted by temperature. Fitted regression lines are shown.
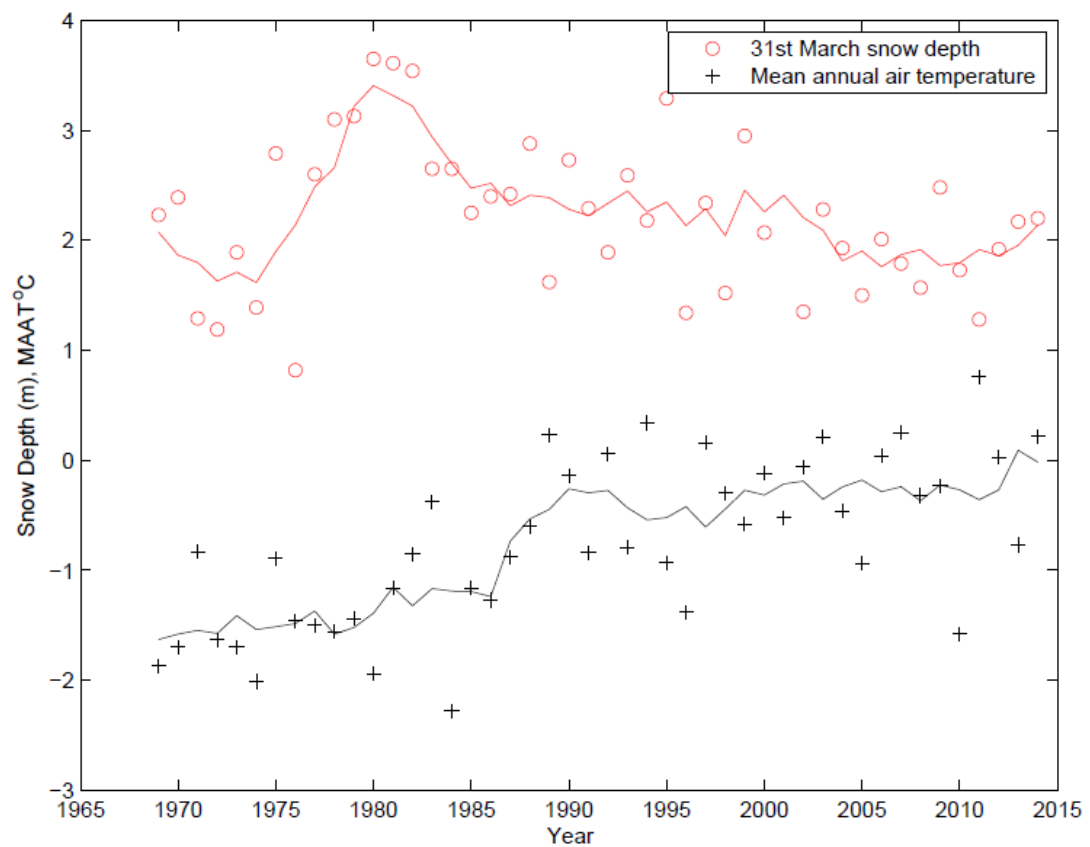
Figure 7. Modelled 31st March snow depth at 2,900 m and mean annual air temperature at Grand Saint Bernard, with 5 year running means shown.